EEET ECOLOGICAL ENGINEERING & ENVIRONMENTAL TECHNOLOGY

Ecological Engineering & Environmental Technology, 2026, 27(7), 186–204
https://doi.org/10.12912/27197050/222552
ISSN 2719–7050, License CC-BY 4.0

Received: 2026.05.17
Accepted: 2026.06.15
Published: 2026.07.01

Structural evolution and deformation control on mineralization in the Central Draâ Sfar copper-zinc volcanogenic massive sulfide deposit (Morocco)

Imad Aflla[1,2*], Abdelfatah El Mostadi[3], Zoubair El Ouad[1], Marieme Jabbour[4], Ali El-Masoudy[2,5], Mustapha Souhassou[1], Outigua Abdelhak[2], Salah Boukerrou[5], Omaima Essoualeh[3], Lhou Maacha[2]

[1] 2GBEI Laboratory, Polydisciplinary Faculty of Taroudant, Ibn Zohr University, Agadir, Morocco
[2] Managem Group, Twin Center, 20000 Casablanca, Morocco
[3] Geodynamic and Geomatic Laboratory Department of Geology, Faculty of Sciences, Chouaïb Doukkali University, EGGPG, B.P. 20, 24000 El Jadida, Morocco
[4] LAGAGE Laboratory, Department of Geology, Faculty of Sciences Ibn Zohr University, 80000 Agadir, Morocco
[5] Applied Geology and Remote Sensing, Moulay Ismail University of Meknes, Faculty of Sciences and Techniques, BP 509, Errachidia Boutalamine, 52000, Morocco
* Corresponding author's e-mail: imad.aflla@edu.uiz.ac.ma

ABSTRACT

The Draâ Sfar polymetallic deposit in the Central Jebilet (Morocco) is a Variscan volcanogenic massive sulfide (VMS) system in which orebody geometry is strongly overprinted by polyphase deformation. This study aims to determine how Variscan tectonic processes have controlled the architecture, distribution, and apparent multiplicity of sulfide lenses in the poorly documented Central Block at ~640 m depth, and to distinguish between primary depositional features and tectonically induced segmentation of mineralization. The study further seeks to evaluate the relationship between deformation, hydrothermal alteration, and metal redistribution within a structurally complex VMS environment. To achieve this, an integrated approach combining drill-core logging, structural analysis, petrography, X-ray diffraction, and whole-rock geochemistry was applied to representative sections of the Central Block. Lithological correlations and deformation fabrics were used to reconstruct orebody geometry, while geochemical indices (AI, CCPI, ISER) were employed to quantify alteration zoning and its spatial relationship to structural domains. The results show that sulfide mineralization occurs predominantly as pyrrhotite-rich lenses associated with chalcopyrite, sphalerite, and pyrite, which are systematically folded, boudinaged, and segmented by ductile shear zones and late brittle faults. The apparent multiplicity of ore lenses is demonstrated to result largely from tectonic duplication of originally continuous mineralized horizons rather than independent depositional centers. Alteration patterns display a clear structural control, with proximal chlorite–carbonate–pyrite assemblages concentrated within high-strain zones and distal sericite-rich halos developed in the surrounding wall rocks, reflecting deformation-enhanced fluid circulation. The paragenetic evolution records three main stages, from syngenetic sulfide deposition to syn-deformational remobilization and late fracture-controlled mineral precipitation. The study is limited by the discrete nature of drill-core sampling and the absence of continuous 3D geophysical constraints, which restrict full spatial reconstruction of ore continuity. Nevertheless, the results provide a robust framework for understanding structurally reworked VMS systems and improve predictability in exploration targeting. This work demonstrates that Variscan deformation is the principal control on orebody architecture in the Central Block of Draâ Sfar, offering a revised genetic model for tectonically modified VMS deposits and providing a transferable approach for interpreting similar deformed sulfide systems in orogenic belts.

Keywords: Jebilet Massif, central Draâ sfar, variscan orogeny, polymetallic sulfide deposits, volcanogenic massive sulfides.

INTRODUCTION

The Draâ Sfar polymetallic deposit, located approximately 13 km northwest of Marrakech, represents one of Morocco's significant base-metal resources. This volcanogenic massive sulfide (VMS) system, enriched in Zn, Pb, and Cu, belongs to the Variscan Jebilet massif in central Morocco. The deposit was first identified in 1953 when the Moroccan Geological Survey Service (SEGM) recognized the iron cap of the Draâ Sfar North sector. Systematic geological exploration and infrastructure development began in 2002, leading to the start of mining operations in 2004.

The deposit is hosted within the Sarhlef series, composed mainly of schists interbedded with sandstone, which gradually transition upward into carbonate-bearing and finer clastic units (Leprêtre et al., 2024). Its Viséan age has been proposed based on palynological analyses (Moreno et al., 2008). However, the stratigraphic framework remains debated, as volcano-sedimentary sequences have been assigned either to the Upper Viséan–Namurian based on Posidonomya becheri occurrences (Huvelin, 1977) or alternatively to the Devonian based on metamorphosed conodont evidence (Lazreq et al., 2021). This uncertainty reflects the complex tectono-sedimentary evolution of the Jebilet domain and highlights the need for structural reassessment of mineralized horizons.

In VMS systems of the Variscan belt, primary stratabound sulfide lenses are commonly modified by later deformation, metamorphism, and fault reactivation, which may significantly obscure original depositional geometries. Although Draâ Sfar is generally interpreted as a syngenetic VMS deposit subsequently overprinted by Variscan deformation, the extent to which current orebody architecture reflects primary volcanogenic controls versus tectonic reorganization remains unresolved.

This uncertainty is particularly critical in the Central Block of the deposit, located at approximately −640 m depth, where previous observations suggest a structural behavior of mineralized lenses that differs from both the southern sector, characterized by a single lens, and the northern sector, where multiple lenses are reported. However, the geometry, continuity, and genetic significance of these contrasting configurations have not been systematically constrained using integrated structural and geochemical data.

The main gap in current knowledge therefore concerns the lack of a unified tectono-metallogenic framework capable of distinguishing between (i) primary multi-center VMS deposition and (ii) tectonic segmentation and duplication of originally continuous sulfide horizons during polyphase Variscan deformation.

Therefore, there is a need to fill this gap by integrating lithological, structural, petrographic, geochemical, and mineralogical data from deep drill cores of the Central Block in order to reconstruct the deformation history of the ore system and its control on sulfide lens architecture and hydrothermal alteration patterns.

We test the hypothesis that the apparent multiplicity of sulfide lenses in the Central Block is primarily the result of tectonic segmentation and duplication of an originally continuous mineralized horizon through D1–D4 deformation events, rather than reflecting independent depositional centers. We further hypothesize that deformation-enhanced permeability along shear zones systematically controlled hydrothermal fluid flow, producing spatially coherent alteration zoning expressed by CCPI, ISER, and AI indices.

The objective of this work is therefore to establish a structurally constrained genetic model of the Draâ Sfar Central Block that links Variscan deformation phases to orebody geometry and alteration distribution, thereby refining the understanding of how polyphase tectonics modifies VMS systems at depth.

GEOLOGICAL SETTING

Jebilet massif

The Variscan Jebilet massif, stretching ~170 km long and 35 km wide between the Bahira plain in the north and the Haouz plain in the south, constitutes a Variscan inlier marked by intense pre- to syn-orogenic magmatic activity (Huvelin, 1977).

The igneous activity is essentially manifested by an ante-tectonic bimodal magmatism, with ~65% mafic rocks (gabbros, LREE-depleted tholeiites) and 35% felsic rocks (tuffs, rhyolites, rhyodacites, andesites, quartz-keratophyres) (Essaifi et al., 2004). Syn-to post-tectonic granodioritic plutons, peraluminous to biotite, are also present, intruding into the schistose and volcano-sedimentary formations (Bouloton, 1992; Lagarde et al., 1992). Finally, late microdioritic dykes cut across the whole complex (Figure 1) (Huvelin, 1977; Bouloton and Gasquet, 1995).

Structurally, the main shear zone, the West Jebilet Shear Zone (WMSZ), separates the Coastal Block (Western Jebilet) from the Central Jebilet (Figure 1). The sedimentary rocks underwent regional epizonal metamorphism accompanied by contact metamorphism linked to granitic intrusions (Michard, 1976; Huvelin, 1977). The structures are characterized by NNE-SSW synschistose folds, S1 cleavage linked to epizonal metamorphism, subparallel shearing, and S2 crenulation cleavage. The shear zones are organized into sinistral (N160°) and dextral (ENE) systems, the latter being associated in particular with the Mesret fault and the Kettara intrusion (Essaifi et al., 2001).

Drâa Sfar deposit

The Draâ Sfar polymetallic deposit is located ~13 km northwest of Marrakech, on the southern margin of the central Jebilet (Figure 1). It is subdivided into three blocks: Draâ Sfar south, center, and north, located on either side of the Tensift River, respectively. The northern block, oriented NS, is characterized by a limited outcrop of the Variscan basement with a cap of altered iron. The southern and central blocks extend south of the Wad-Tensift for ~1.2 km in length and 700 m in width, emerging in the Mesozoic-Cenozoic Miocene-Pliocene and Quaternary formations.

The mineralization occurs as sulfide lenses hosted between a volcanic to volcano-sedimentary footwall series with tuffaceous facies and a detrital hanging wall series with fine pelites. The local stratigraphic series thus consists of three units: the footwall unit, the mineralized middle unit, and the hanging wall unit (Figure 2).

MATERIALS AND METHODS

For the purpose of examining and emphasizing the connection between Variscan deformation and tectonometallogenetic evolution that led to the formation of mineralization at Draâ Sfar deposit, this study is primarily based on: (i) analysis of the structural data gathered both from underground mining levels and drill core samples; (ii) metallographic studies performed on the thin sections cut and polished at the REMINEX Research Center along with the petrographic studies carried out on the host rock samples in order to establish the mineralogy and petrography of the rocks; and (iii) geochemical studies related to hydrothermal alteration.

Studies of structural data have been performed on the −632 m sublevel inside the mining shafts of the Draâ Sfar Central Block. The studies included measurements from the drilling cores. Structural analysis has been aimed at mapping faults, schists, folds, shear-related fabrics, and deformation structures that influenced host rocks as well as mineralization zones. More than several hundred structural measurements have been made underground, defining deformation phases influencing the ore deposit. This paper describes the major structural features corresponding to the various stages of deformation within the deposit. Detailed structural

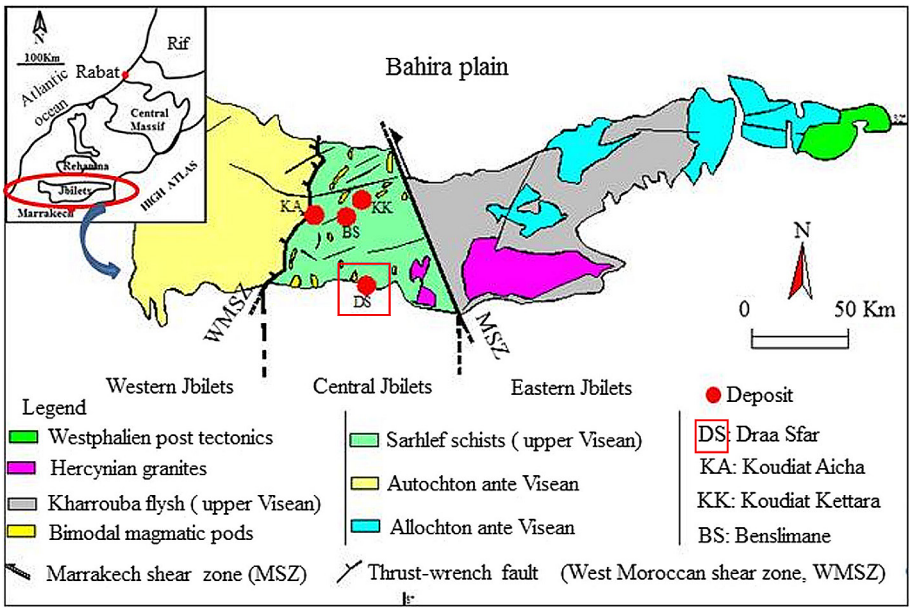

Figure 1. Location of the main sulfide deposits in central Jbilets modified, after Huvelin (1977)

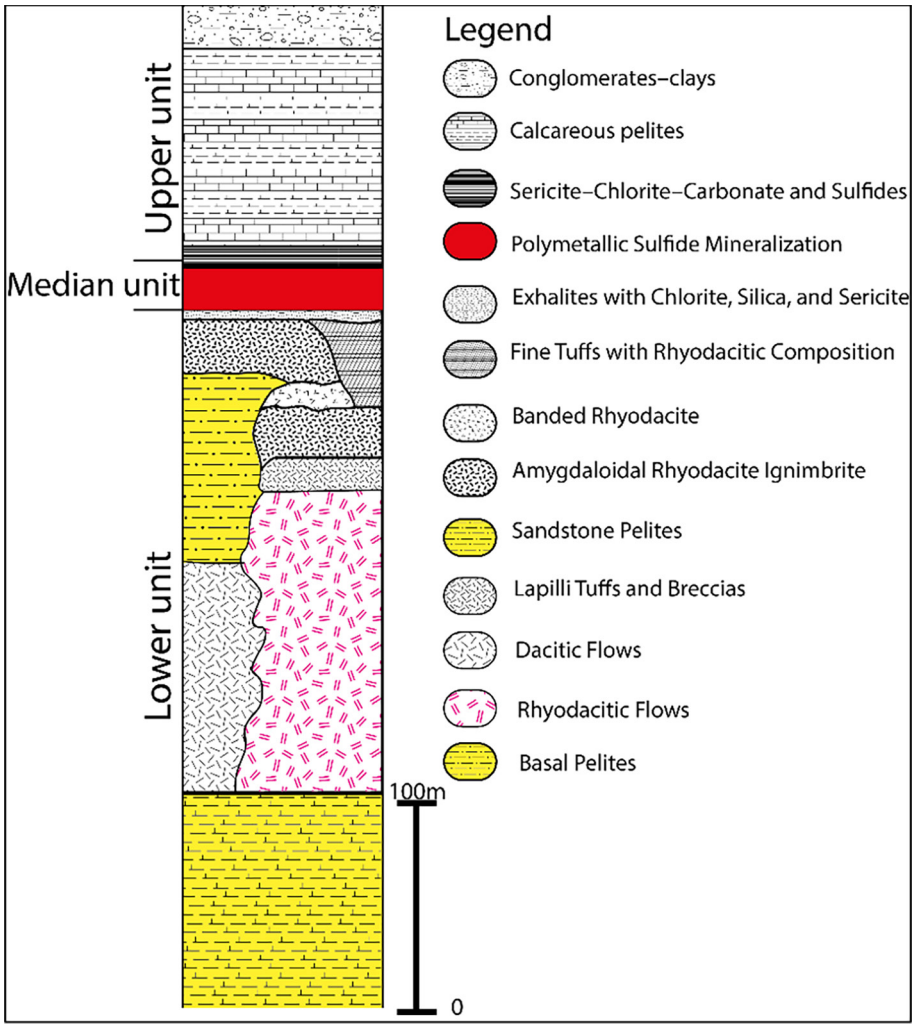

Figure 2. Representative lithostratigraphic log of the Draâ sfar deposit, modified after ben aissi (2008)

measurements and field photographs are provided in the Supplementary Materials.

The drill cores, namely DF462, DF453, DF469, DF463, and DF471, were chosen from the Central Draâ Sfar Block on the basis of lithological completeness of these drill holes. The above-mentioned drill holes crosscut all the stratigraphic horizons that contain the ore bodies and allow one to examine tectonic structures associated with the Variscan deformation stages owing to good visibility and continuity of cross-sections of these rock formations. The drill hole DS98 (X = 240728.500, Y = 127856.000, Z = -15.500) was chosen for geochemical studies due to the typicality of this point relative to the studied drill holes and complete exposure of the lithology from the hanging wall to the footwall succession. In contrast to other drill holes, where geochemical sampling was conducted mainly in mineralized horizons, DS98 is the only drill hole where complete sampling was done along the whole exposed lithological sequence.

Geochemistry

The drill core from borehole DS98 was thoroughly logged and continuously examined from the beginning to the end of the drill hole, with particular attention given to lithological variations, contacts, hydrothermal alteration zones, and mineralized intervals. A total of 41 whole-rock samples were collected along the drill hole, with sampling carried out at each remarkable lithological variation and contact in order to characterize the different lithological units, hydrothermal alteration zones, and mineralized intervals intersected in DS98. Among these, 31 samples correspond to footwall fotmations collected from depths ranging between −15 m and −190 m (samples E1–E31). The first massive sulfide lens (sample E24) occurs between −150 m and −152 m within this lithological unit. The second mineralization zone (sample E32) is located between −190 m and −191.5 m. This interval

marks the transition into the hanging wall formations (−191.5 m to −236 m; samples E33–E41).

Geochemical analyzes were conducted at the REMINEX lab (Marrakech, Morocco) and were based on a joint use of analytical procedures of four-acid digestion followed by analyses using ICP-AES and ICP-MS. Major element compositions were analyzed by means of ICP-AES following analytical procedure CR/AN/MO/111.00, while trace element compositions were determined by ICP-MS according to analytical procedure CR/AN/MO/70.00. The study of major element geochemistry included peroxide fusion of pulverized samples in order to dissolve refractory minerals.

Quality assurance and quality control (QA/QC) protocols for data analysis were followed as per laboratory norms. Approximately 10% of the analysis comprised duplicate analysis to check reproducibility, 5% constituted analytical blank analysis to check for contamination, and 2.5% of the whole analysis comprised certified reference materials (standards). Reproducibility for the analysis was around ±5% for major elements and ±10% for minor elements. Detection limits differed from element to element depending on the method of analysis, and these details are presented in the Supplementary Materials.

The geochemical characterization of hydrothermal alteration was carried out using the collected samples from drill hole DS98 (in the Supplementary Materials). Alteration indices were computed from major-element data, including the chlorite index (ICHLO) Equation 1, the sericite index (ISER) Equation 2, the Ishikawa alteration index (AI) Equation 3, defined by Ishikawa et al. (1976), and the chlorite-carbonate-pyrite index (CCPI) Equation 4, of Large et al. (2001). These indices were selected because they are widely used in volcanogenic massive sulfide (VMS) systems to characterize chloritic, sericitic, and carbonate hydrothermal alteration halos associated with sulfide mineralization.

$$ICHLO = 100 \times (Fe_2O_3 + MgO) / (Fe_2O_3 + MgO + 2CaO + 2Na_2O) \quad (1)$$

$$ISER = 100 \times K_2O / (K_2O + Na_2O) \quad (2)$$

$$AI = 100 \times (MgO + K_2O) / (MgO + K_2O + Na_2O + CaO) \quad (3)$$

$$CCPI = 100 \times (MgO + FeO) / (MgO + K_2O + Na_2O + FeO) \quad (4)$$

In order to investigate the degree of variation and importance of the effect of hydrothermal alterations in the different geological formations, an ANOVA-type statistical procedure was performed using the alteration indices. It allowed for the determination of the degree of alteration and its variation among the geological formations cut by borehole DS98. All statistics are shown in Supplementary Materials.

Mineralogy

Seven samples were collected for petrographic analysis to characterize the mineralogy and petrography of the host formations. These samples were prepared as thin sections at the REMINEX laboratory, and microscopic observations were carried out using an OLYMPUS CX31 optical petrographic microscope. The remaining samples were ground into powders for mineralogical investigations and prepared at the Department of Geology, Faculty of Sciences of El Jadida, Morocco.

X-ray diffraction (XRD) analyses were conducted on the powdered samples at the Chemistry Department of the Faculty of Sciences of El Jadida using a Bruker D8 Advance Twin diffractometer equipped with a copper anode ($CuK\alpha_1$ radiation, $\lambda = 1.5418$ Å). Diffraction patterns were acquired over a 2θ range of 5–80° with a step size of 0.02°. Prior to analysis, all samples were finely ground in an agate mortar.

In addition, ten ore samples from the Draâ Sfar Central zone were selected for metallographic analysis. Polished sections were prepared at the REMINEX laboratory, ore mineral assemblages and textures were examined using an OLYMPUS BX53M reflected-light metallographic microscope.

The combined petrographic, mineralogical, and metallographic analyses allowed the identification of primary and secondary mineral phases in both host rocks and ores, as well as the reconstruction of their paragenetic relationships.

RESULTS

Field observations

The results of drilling core observations demonstrate the vertical lithological zonation, geometry of sulfide lenses, and contacts of sulfide lenses and host-rocks formations (Figure 3). Three drilling cores (DF462, DF453, and DF469) were

logged in detail on a 1:50 scale with an objective to record lithological differences, structural properties, intensity of alteration and presence of sulfides in Draâ Sfar Central VMS deposits.

The hanging wall part (−632 to −794 m) in drill core DF462 (−632 to −884 m) is characterized by regular alternation of black pelites, light-colored sandstones, and darker pelites (Figure 3). Such rocks are altered (chloritization) with some local crushing effects along with quartz-chlorite veins. Secondary S2 cleavage occurs in zones of S1 foliation. In the first sulfide lens (−802 to −821 m) the main type of sulfides is represented by massive sulfides (pyrrhotite) with admixtures of chalcopyrite, pyrite, and sphalerite.

Drill core DF453 (−631 to −884 m) exhibits a hanging wall section (−631 to −833 m) composed of schistose black pelites characterized by a well-developed S1 foliation dipping between 0° and 35° (Figure 3). Quartz–chlorite veins and disseminated pyrite–chalcopyrite mineralization are locally observed. The sulfide lens between −833 and −844 m consists of massive pyrrhotite with minor chalcopyrite and pyrite. Below this interval, the footwall (−844 to −884 m) is composed of chloritized sandy pelites interbedded with folded sandstone layers and a thin volcanic tuff horizon (~30 cm thick).

In drill core DF469 (−632 to −1036 m), the hanging wall (−632 to −813 m) consists of black pelites showing progressive chloritization and deformation with depth. Deformed quartz veins are common throughout this interval. Between −740 and −794 m, S2 crenulation cleavage and kink-band microfolds are locally developed. Three sulfide lenses are identified at −813 m, −910 to −913.7 m, and −917.5 to −956 m, the latter reaching a thickness of approximately 44 m. Below −956 m, the footwall consists of chloritized sandy pelites and volcanic tuffs, with sharp and locally faulted contacts with sulfide bodies (Figure 3).

Structural analysis

The Draâ Sfar deposit shows complex tectonic deformation affecting both mineralized formations and surrounding rocks (Michard et al., 2010; Poucl et al., 2017). Structural interpretations are based on drill core observations and field data presented in Figures 4–6. The deformation history is characterized by ductile and brittle regimes that record progressive tectonic evolution.

Ductile deformation

Three phases of ductile deformation (D1, D2, and D3) are recognized in the study area. The earliest deformation phase (D1) corresponds to the main syn-metamorphic compressive event

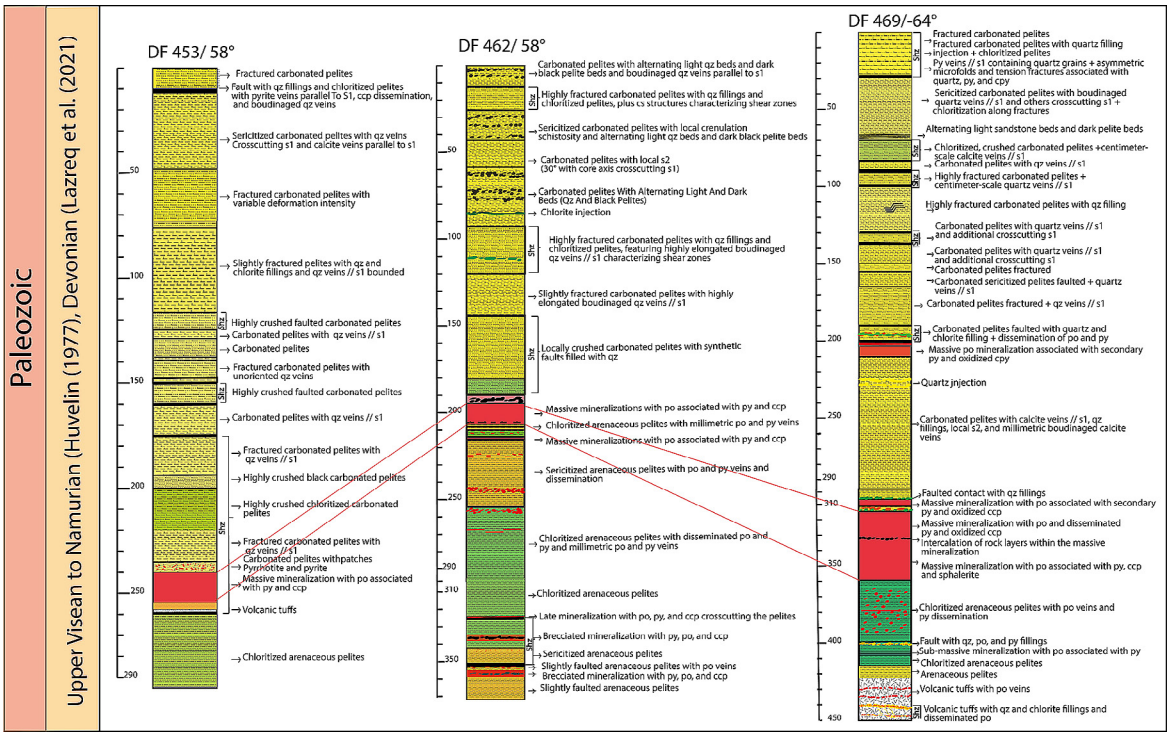

Figure 3. Correlation of the stratigraphic logs of the three cored drill holes DF353, DF462, and DF469

of the Variscan orogeny. It generated P1 folds and a pervasive S1 foliation developed under greenschist-facies conditions (Figures 4A, 4B; Figures 5A, 5B). Primary bedding (S0) is commonly strongly transposed into S1, resulting in an apparent parallelism between S0 and S1 and making recognition of original layering difficult, particularly in homogeneous lithologies.

The S1 foliation generally strikes sub-meridionally and dips steeply to the east (~75°E) (Figure 4B1). In black pelites, S1 is expressed as a well-developed flow cleavage defined by the preferred orientation of white mica (Figure 5B). At microscopic scale, quartz veins exhibit P1 microfolds whose axial planes are marked by elongated white mica aggregates (Figure 5A). Within ore lenses, S1 is recorded by the stretching of sulfides and gangue minerals as well as microfolding within massive ores (Figure 5C). This deformation stage was accompanied by syn- to late-tectonic contact metamorphism related to the emplacement of the Bamzga, Tabouchent, and Ouled Ouaslam granodioritic intrusions (Mrini et al., 1992).

The second phase of deformation (D2) involved ductile shearing and boudinage of mineralization lenses and quartz veins (Figure 4C). Pressure solution features and pressure shadows of quartz clasts in thin section indicate simple shear deformation that accounts for stretching and segmentations in quartz veins (Figure 5D).

The third phase of ductile deformation (D3) resulted in a crenulation cleavage (S2), which is oriented along the WNW-ESE trend and plunges at an angle of 75–80° to the south-southwest direction (Figures 4D, 4E). The S2 cleavage is most clearly expressed in the pelitic hanging walls, and represents late compressional reorientation of pre-existing fabrics in accordance with Variscan trends identified in the region (Michard et al., 2010; Poucl et al., 2017).

Brittle deformation

The brittle structures overlay the ductile structure and are comprised of tension gashes and several sets of strike-slip fault zones (Figure 4F; Figure 6). These structures correspond to late-stage transpressional deformational style affecting the area (Saber, 1998; Zouicha et al., 2022; Yaagoub et al., 2023).

The tension gashes occur as open space quartz veins striking approximately NNE (Figure 4F), which corresponds to extensional phases of transpressional deformational regimes.

Three major fault sets can be recognized. First, the N–S to NNE–SSW trending faults dip ~75°E and are mostly sinistral in nature as shown in drill cores as quartz veinlets striking NE-SW (Figures 6A, 6B). Second, the E–W to ESE–WNW faults dip ~70°S and are dextral in strike-slip movement (Figure 6C). Third, the NE–SW faults dipping ~75° SE are dextrally oriented but show occasional displacement of S1 foliation and quartz veins (Figure 6D).

Geochemistry and hydrothermal alteration

Geochemical investigations provide essential insights into the processes controlling mineralization, alteration, and the evolution of volcanic-hosted massive sulfide (VMS) deposits. This research employs a geochemical perspective to define the intensity and characteristics of alteration, map the distribution of essential elements linked to mineralization, and establish a framework for understanding the paragenetic and tectono-metallogenic development of the Draâ Sfar Central VMS deposit.

Variation of major elements

The geochemical characterization of alterations in the Draâ Sfar Central Block was carried out on core drilling samples (DS98; Figure 7A, Table 1 in the supplementary data). Samples were classified according to their position within the formations intersected by the drill hole (Figure 7A). The aim of this study is to define the dominant type of hydrothermal alteration and to estimate its intensity by applying the simple element ratio method (Gaboury, 2004), which relies on the variations of major-element composition relative to immobile components.

As can be observed from the results of the geochemical investigation performed along drill hole DS98 (Figure 7A), there is significant difference between the host rock formations and mineralization zones. There is a sharp distinction concerning major element concentrations between host rocks and ore zones in terms of chemical content along drill hole DS98. While SiO_2 in host rocks varies between ~30–64 wt.%, Al_2O_3 contents vary between ~13–18 wt.%. Within ore zones, SiO_2 is significantly reduced to levels below 20 wt.%, and even below 0.5 wt.% locally, and Al_2O_3 content

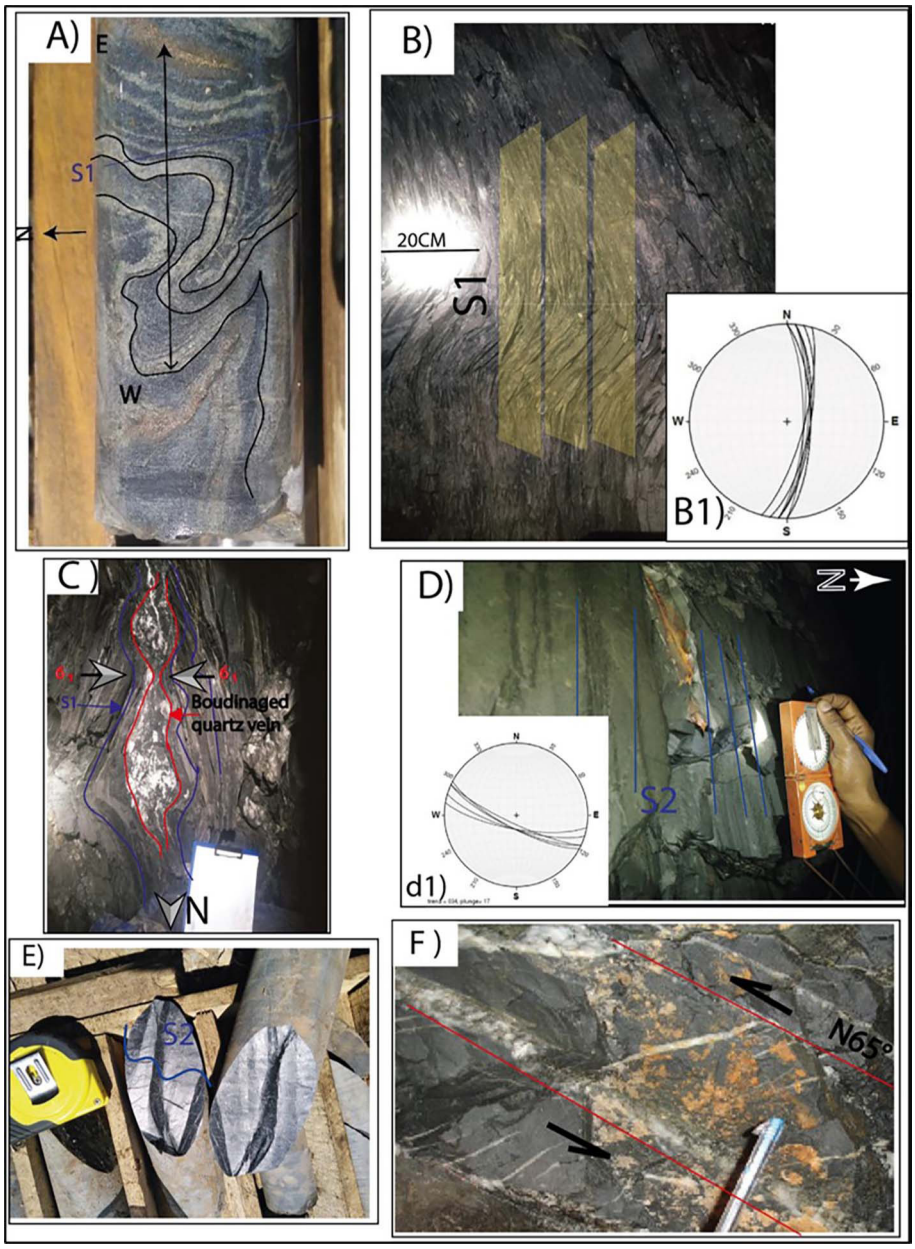

Figure 4. Variscan deformation in the terrains of Central Draa Sfar: A) P1 folds with a general NNE-SSW orientation, crosscut by borehole DF453. B) Black pelites at the bottom (level -726 m) affected by S1 cleavage. B1) Cyclographic diagram showing the orientation of S1 cleavage planes. C) Boudinaged quartz vein molded by S1 cleavage within the black schistose pelites D) Crenulation cleavage (S2) D1) Cyclographic diagram showing the orientation of S2 cleavage planes E) S2 cleavage affecting the black pelites of the hanging wall at the core scale. F) Tension gashes with quartz filling within the Hanging-wall formations

is significantly reduced to about 1–2 wt.%. Fe_2O_3 in host rocks varies between 5–26 wt.%, while Fe_2O_3 in mineralized zones reaches levels of ~58–80 wt.%. While CaO concentrations are fairly low in host rocks (~2–5 wt.%), with a few instances of enrichment to levels up to 12–13 wt.%, within mineralized zones, CaO is fairly low (<2 wt.%). Host rocks have low concentrations of MgO and K_2O (~1–5 wt.% for MgO and ~1–4 wt.% for respectively) but are strongly depleted in the mineralized intervals, where K_2O may fall to ≤0.15 wt.%. MnO and Na_2O remain consistently low along the drill hole, generally <0.3 wt.%, and are nearly absent within the mineralized zones. These concentration ranges document a clear geochemical contrast between host rocks and ore-bearing intervals, as illustrated in Figure 7B.

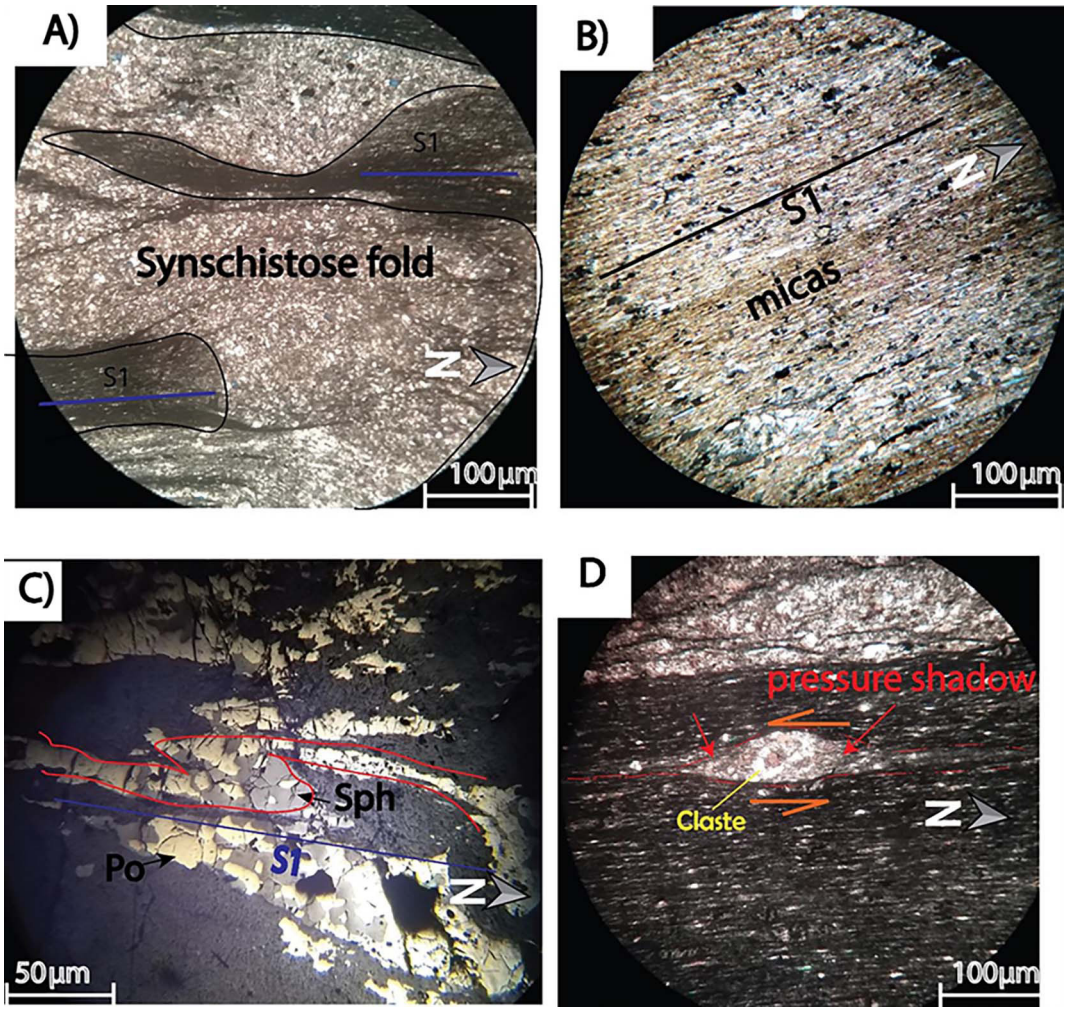

Figure 5. Variscan deformation phases at the microscopic scale from drill core DF543. (A) Thin section observed under plane-polarized light (PPL) showing P1 folding of mica minerals in black pelites. (B) Thin section under polarized light showing schistosed black pelites with schistosity defined by the alignment of mica minerals (sericite and muscovite). (C) Polished section observed under metallographic microscopy from the mineralized zone showing P1 folding of sphalerite grains within the sulfide assemblage. (D) Thin section under plane-polarized light showing pressure-solution structures and the development of pressure shadows around a quartz clast. Mineral abbreviations: Po = pyrrhotite, Sph = sphalerite, S1 = schistosity

Alteration indices (AI, ICHLO, ISER, CCPI)

The highest values of the ICHLO index are found in the mineralized bodies with an average value of 95.63%, while lower average values can be found in the footwall (69.2%) and hanging wall (70.4%) formations (Figure 7C). The ISER index indicating sericite abundance. Higher ISER indices were found in footwall formations (98.4%), then in hanging walls (53.04%), while the lowest average ISER indices can be found in mineralized bodies (19.37%) (Figure 7C).

According to Gaboury (2004), the slightly altered rocks normally have Ishikawa alteration index (AI) within 20 and 40. The Ishikawa alteration index on drill hole DS98 changes significantly with depth. Alteration is most intense in footwall formations where the average AI value equals 63.88%, in hanging wall formations, AI equals 53.04%, whereas the AI value for mineralized zones is less than 20. These findings coincide with the findings from petrography, where intense hydrothermal alteration is identified in the footwall with sericite-chlorite paragenesis, while the massive sulfide lenses consist predominantly of ore minerals with minor alteration to silicates.

The CCPI value is quite similar for both the mineralization and hanging wall (99.93% and 91.57%, respectively) when contrasted to the value for the footwall (82.16%). The above results

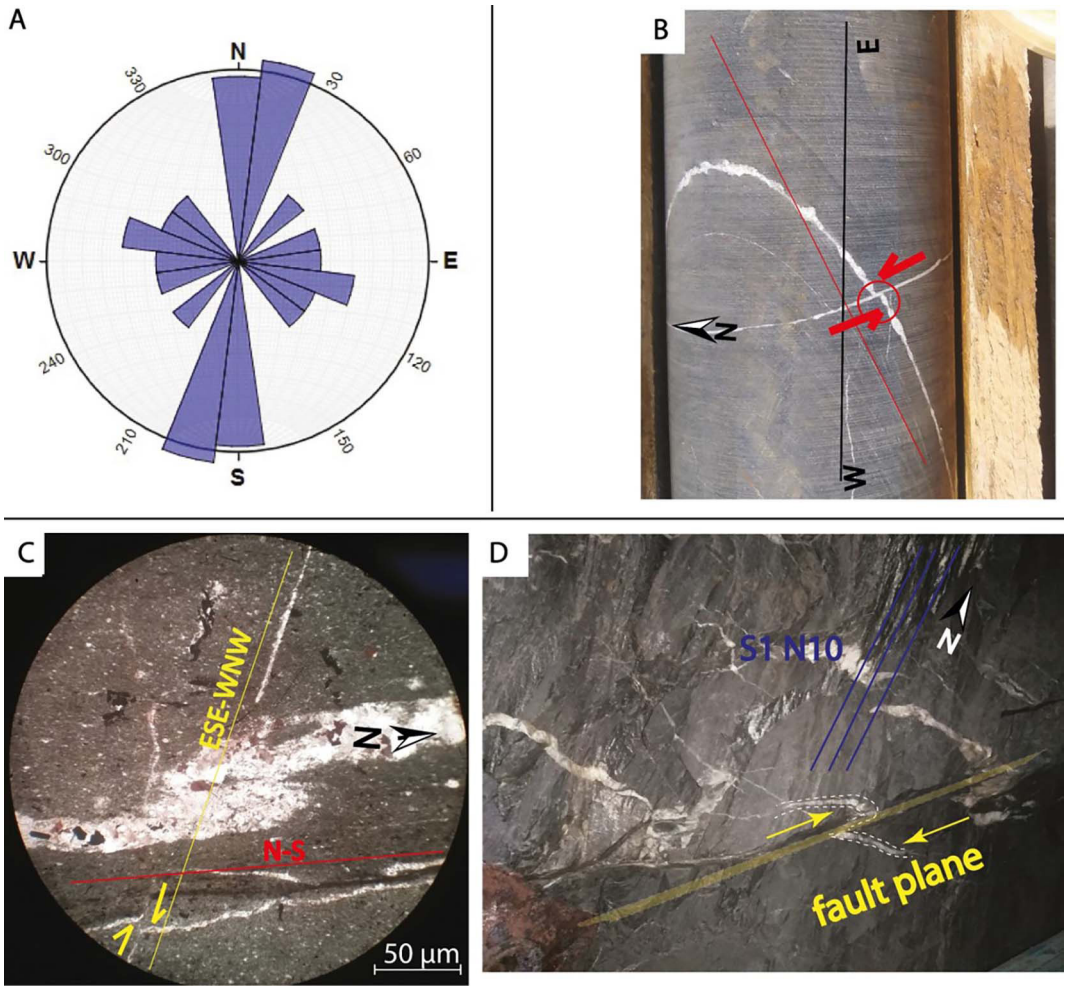

Figure 6. Brittle deformation phases of Central Draa Sfar, A) Directional rose diagram showing the main orientations of different fault systems related to this deformation, B) N-S fractures with quartz infill displacing NE-SW fractures with a sinistral, movement, C) ESE-WNW quartz-filled fractures crosscut the N-S fractures of Family 1 with a dextral movement. D) fault trending N45

are consistent with the findings obtained from petrographic studies, which revealed the presence of chlorite, carbonate minerals (dolomite, ankerite, and siderite), and sulfides in the ore zone and hanging wall black pelite rocks, while they are not common in the footwall rocks (Figure 7C).

Effect of deformation on hydrothermal alteration

Previous studies (Lagarde, 1985; Mrini et al., 1992) indicate that the massif underwent pervasive hydrothermal alteration contemporaneous with Variscan deformation and the formation of sulfide mineralization around 301 ± 15 Ma (Rb-Sr dating on biotite). In the Central Block, alteration intensity systematically increases near ductile shear zones, highlighting a structural control on fluid circulation. A "Box Plot" alteration diagram (Figure 8), comparing the Ishikawa index (AI) and the chlorite-carbonate-pyrite index (CCPI), shows a positive correlation, indicating a gradual increase in both sericite and chlorite alteration toward zones of higher strain. This pattern suggests that deformation enhanced rock permeability, promoted hydrothermal fluid flow, and consequently intensified alteration in the vicinity of shear zones.

Mineralogy and paragenesis

Petrological characteristics and X-ray diffraction analysis of the host rocks

The hanging wall pelitic rocks are characterized by their black color, tuffaceous nature, and fine-grained character (Figure 9A). Petrographic studies showed that they have a granolepidoblastic texture associated with schistosity, in which

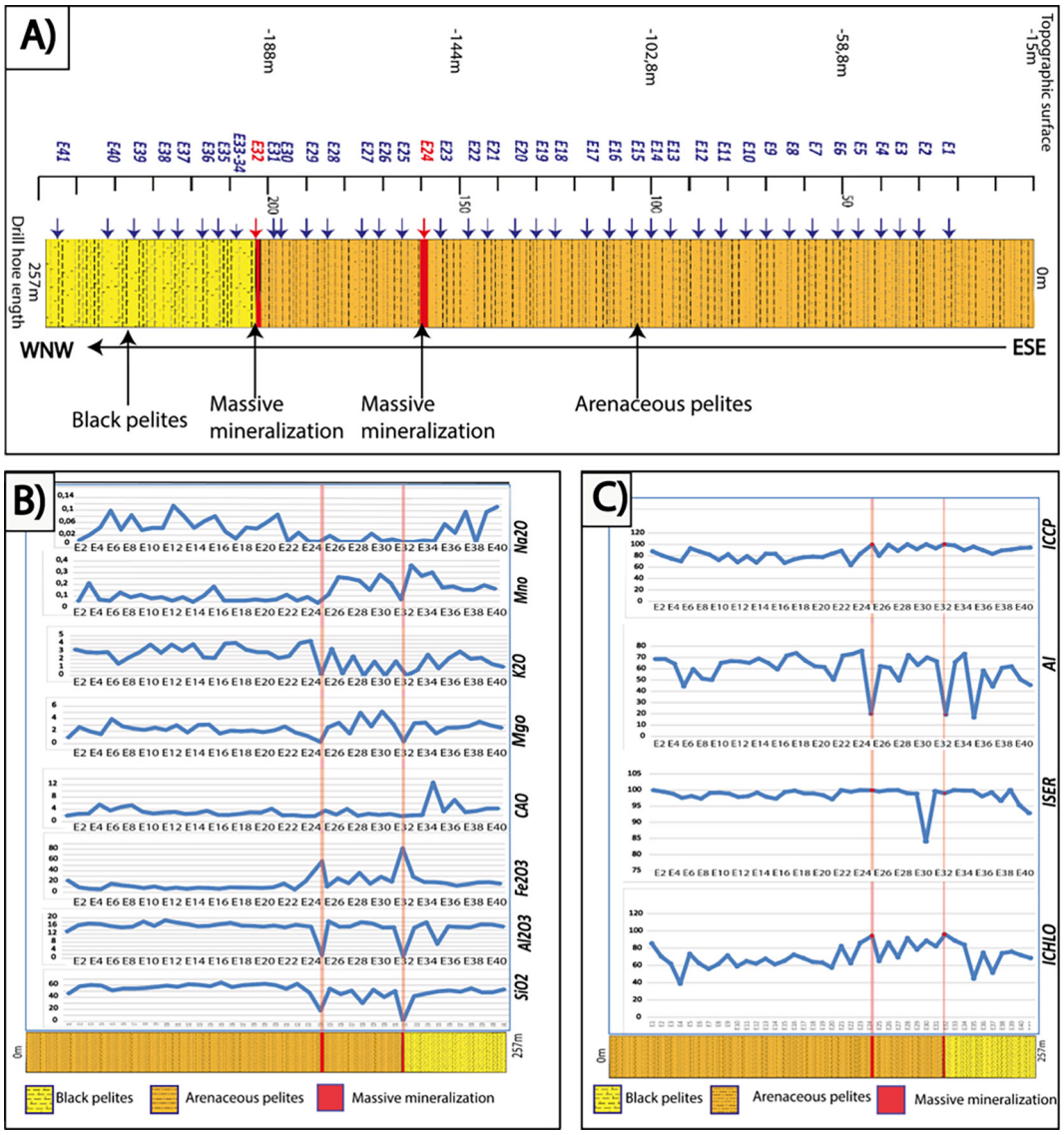

Figure 7. A) Variations in major elements in core sample DS98.
B) Variations in major elements in core sample DS98.
C) Représentation des indices d'altération en fonction de la profondeur dans le sondage DS98

equant and prismatic quartz grains are dominantly oriented along the S_1 foliation (Figure 9-A1 and A2). Sericite and muscovite give rise to a planar texture due to their parallel orientation. The rock mineralogy of quartz, Mg-chlorite, muscovite, sericite, and tourmaline suggests greenschist facies metamorphism at low temperatures. The XRD study of a drill core sample from the "carbonate pelites" layer (DF462, 128 m depth) indicated the occurrence of quartz, muscovite, and magnesium calcite (Figure 10A).

The footwall gresopelitic rocks are typically cut by quartz veins in open space fissures and characterized by a fine to medium-grained rock fabric (Figure 9B). Based on the petrographical studies, grano-lepidoblastic to lepidoblastic structures are observed with marked schistosity (Figure 9B1). Multiple generations of mineralization suggest polyphase deformation and metamorphism. There are three generations of quartz, namely pre-kinematic (Qz1), syn-kinematic (Qz2), and post-kinematic (Qz3), while there are two generations of chlorite, syn-kinematic (Chl1) and post-kinematic (Chl2). Tourmaline occurs pre- to syn-kinematic, while muscovite and sericite show syn-kinematic mineral growths. The opaque mineral assemblages are mostly sulfides and have a syn- and post-kinematic occurrence. XRD analysis of sample DF462 (362 m depth) confirms an assemblage dominated by quartz, chlorite, and muscovite, typical of low-grade greenschist facies metamorphism (Figure 10A, B).

Mineralization: morphology and sulfide mineralogy

Previous studies, particularly (Barrakad et al., 1977), indicate that the Draâ Sfar deposit is a polymetallic VMS-type system dominated by pyrrhotite, associated with chalcopyrite, sphalerite, galena, and pyrite. Our observations on drill cores DF462, DF453, DF469, and DF463 reveal that the mineralization occurs mainly in submassive, brecciated, and disseminated forms (Figure 11). Massive and submassive ores are dominated by pyrrhotite, with decreasing abundance of pyrite, sphalerite, and chalcopyrite (Figure 11A, B). Brecciated ore is mainly observed at the contacts of mineralized lenses with host rocks (Figure 11C, D), while disseminated mineralization, the most widespread form, consists of pyrrhotite and chalcopyrite grains uniformly distributed within hanging wall and footwall pelites (Figure 11E). Secondary mineralization is localized in vein fillings along late fractures cutting the primary ore.

The petrography study (Figure 11-A1 to E1) has shown that the pyrrhotite minerals exist in massive, semi-massive, or elongated shapes along the S1 cleavage planes. It often exists in association with the chalcopyrite and the secondary sphalerite minerals. Chalcopyrite appears as inclusions in pyrrhotite or as relics, and the assemblage is sometimes crosscut by host rock beds (Figure 11B1, C1). Late-stage, well-crystallized pyrite accompanies pyrrhotite, chalcopyrite, and galena in the massive sulfide ores (Figure 11D1). Fine disseminations near the host-rock formations mark the onset of mineralization (Figure 11E1).

Based on microscopic analysis of polished sections, the paragenetic sequence related to cleavage development is established, with detailed relationships between ore minerals summarized in (Figure 12).

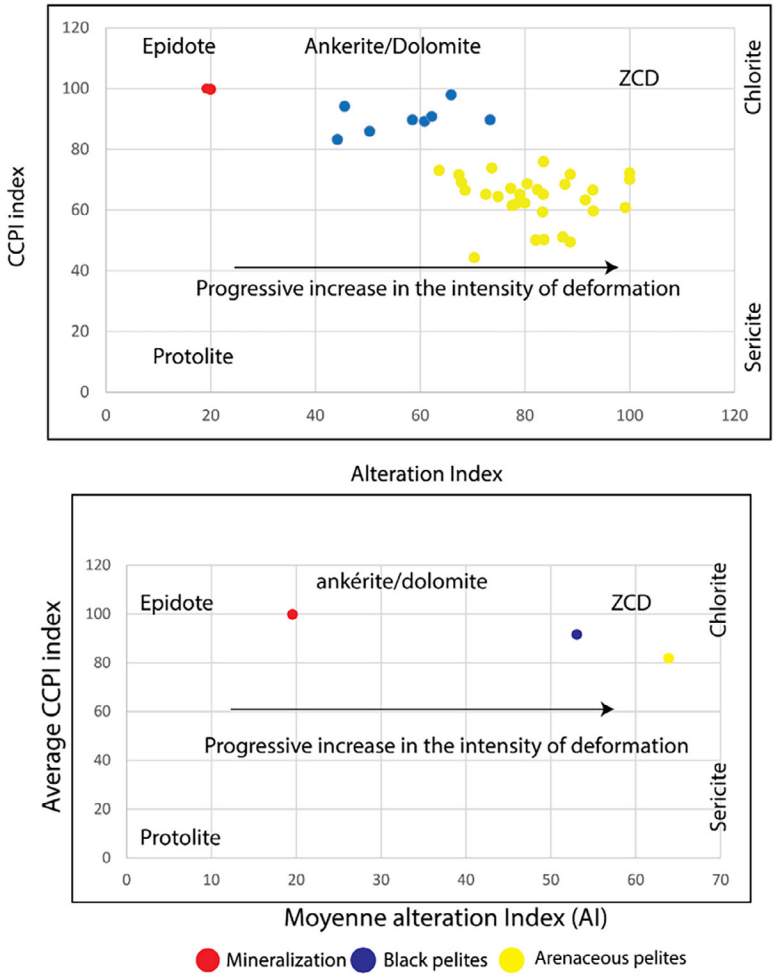

Figure 8. Evaluation of the effect of progressive deformation on weathering affecting the study area in the Box Plot weathering diagram

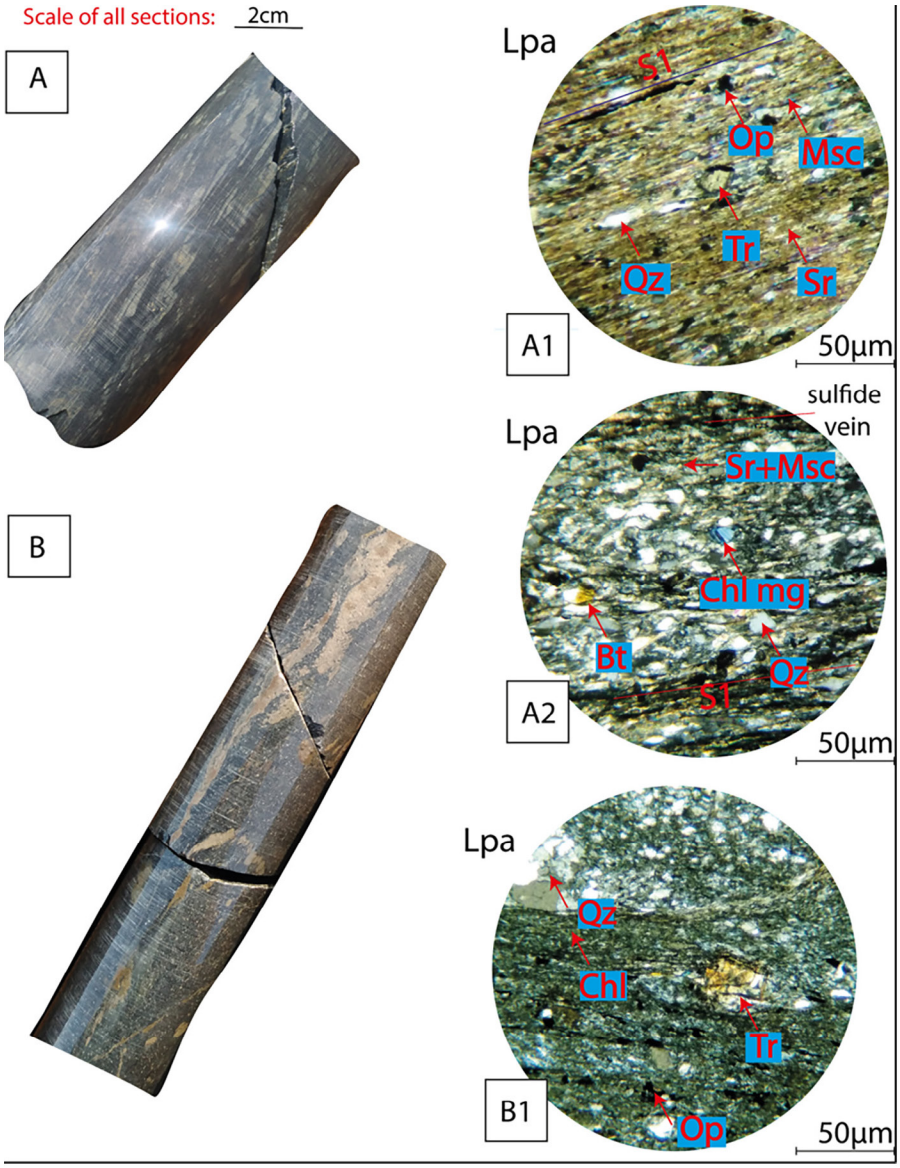

Figure 9. A) Macroscopic aspect of the hanging wall pelites; A1 and A2) Photomicrograph of hanging wall pelites (LP); B) Macroscopic aspect of the footwall sandy pelites; B1) Photomicrograph of the footwall sandy pelites (LP);. Abbreviations: Qz: quartz; Mus: muscovite; Tor: tourmaline; Chl mg: magnesian chlorite; Op: opaque minerals; Ser: sericite; LP: crossed polarized light

DISCUSISON

Structural controls on orebody architecture

The new litho-structural data from drill holes DF462, DF453 and DF469 reveal how the Variscan deformation reorganized the primary syngenetic architecture of the Central Draâ Sfar orebodies. In all three holes, the hanging-wall black pelites carry a pervasive S1 flow cleavage (NNE-SSW with steep eastward dips), locally overprinted by S2 crenulation, while the footwall sandy pelites are less pervasively foliated, consistent with their higher mechanical competence. This property accounts for the easier identification of S1 within the hanging wall structure and the common presence of lenses parallel to S1 at a core scale. The occurrence of faulted contacts on lenses' edges (-813 m and -956 m in DF469; -802 to -821 m in DF462) demonstrates that lens contacts are not solely stratigraphic but also tectonized. A polyphasic deformation history is recorded by the macroscopic fabric of boudinaged quartz vein structures under control of S1, chloritization with crushed bands, and S2 kinking with kink-bands.

An early D1 (syn-metamorphic) compression produced S1 and P1 folds; D2 ductile shearing then localized strain that boudinaged both the host

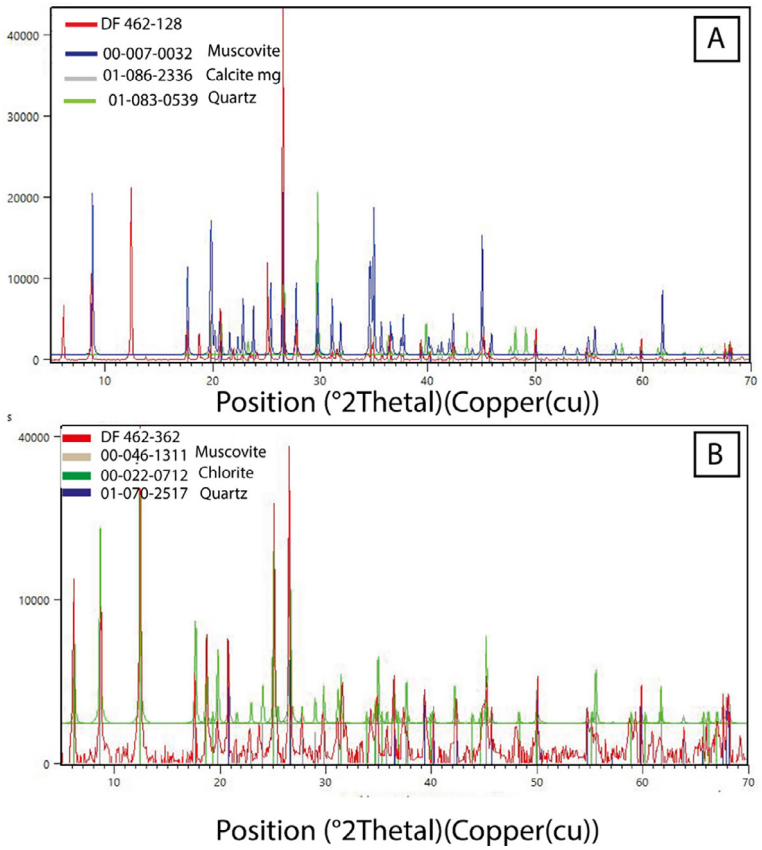

Figure 10. A) X-ray diffraction analysis of the hanging wall pelites (borehole DF462, depth: -128 meters), B) X-ray diffraction analysis of the footwall sandy pelites (borehole DF462, depth: -362 meters)

rocks and the massive sulfides; and D3 added an S2 crenulation trending WNW-ESE. The conjugate strike-slip faults resulting from the late Variscan D4 phase are oriented NE-SW (sinistral) and NW-SE (dextral) with associated tension gashes. This sequence provides a straightforward explanation for the "one lens in the south vs three lenses in the north" problem discussed for the deposit: part of the apparent lens multiplication can arise from tectonic segmentation (duplication and stepover of a single syngenetic body by D1-D2-D4), while genuine multi-center deposition cannot be excluded in such a volcanosedimentary setting. The repetition of massive pyrrhotite lenses and the recurrence of "same lens crossed twice" geometries (e.g., DF462 lenses 3–4; DF469 lenses 1 and 3) are typical signatures of fold-and-shear duplication in deformed VMS systems.

Two operational corollaries follow. First, crossing two "separate" massive intervals does not automatically imply two independent lenses; in Central Draâ Sfar, folded/offset segments of the same lens are plausible where S1-parallel orebodies are intersected obliquely by drilling. Second, the most persistent indicators of lens continuation are (i) alignment with S1 in the hanging wall, (ii) proximity to D2 shear zones, and (iii) the presence of late brittle structures acting as relays a trio that should guide 3D correlation and targeting.

Hydrothermal alteration zoning and its link to deformation

The structural framework described above exerted a first-order control on hydrothermal fluid circulation and alteration patterns.

The major elements on DS98 profiles combined with alteration indices (AI, ICHLO, ISER, and CCPI) reveal a clear asymmetric alteration halo. SiO_2 and Al_2O_3 values are high in the barren host rock but sharply drop, even disappearing, in the massive sulfides, while Fe_2O_3 significantly rises from~15% to~80% corresponding to iron sulfides mineralization. Both K_2O and MgO have moderate amounts in both structural blocks, decreasing towards the mineralization zone, whereas Na_2O is consistently low, which is characteristic of sodium leaching prevalent in VMS alteration systems.

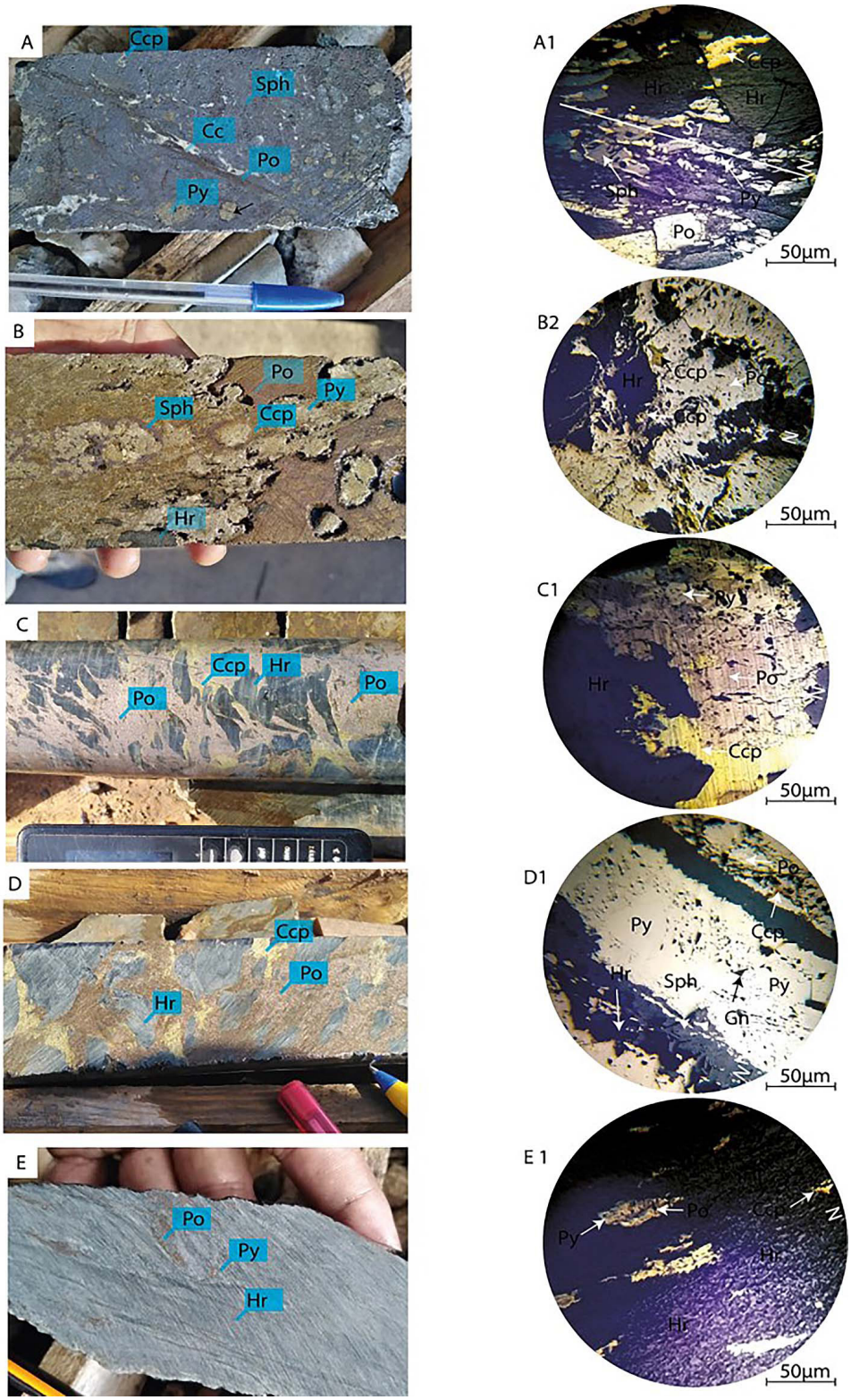

Figure 11. A) Massive sphalerite associated with secondary pyrite and pyrrhotite filling; B) Massive ore with primary pyrrhotite associated with sphalerite and secondary pyrite; C and D) Brecciated ore associated with pyrrhotite, disseminated chalcopyrite, quartz, and host rock elements; E) Example of pyrrhotite dissemination within the footwall formations; A1) Schistosity S1 manifests itself in the elongation of the sphalerite and pyrrhotite veins. Well-crystallized late pyrite; B1) Sub-massive pyrrhotite mineralization associated with chalcophyrite and elements of the host rock; C1) Pyrrhotite, pyrite, and chalcopyrite within the host rock formations; D1) Fracture within primary pyrrhotite filled with secondary pyrite, sphalerite, and galena. Abbreviations: Po: pyrrhotite; Py: pyrite; Ccp: chalcopyrite; Sph: sphalerite; Qz: quartz; Gn: galena; Hr: host rock

The alteration indices clearly corroborate the above trend. For example, the value of ICHLO index (chlorite index) is very high inside the ore body (mean value ~95.6%)

The ISER index (sericite index) is highest in the footwall (~98.4%), lower in the hanging wall (~53%), and lowest in the ore (~19%), demonstrating that sericitization is concentrated in the footwall sandy pelites and decreases upward toward the hanging wall. The Ishikawa alteration index (AI) exceeds 40% in the footwall (mean ~63.9%) and 53% in the hanging wall, both above the "slightly altered" range of 20–40%, while it drops below 20% within the ore consistent with the depletion of mobile Ca-Na and enrichment in Fe-Mg within the massive sulfides. While the CCPI index, integrating chlorite, carbonate, sericite, pyrite, and iron oxides, is highest in the ore (~99.9%) and elevated in the hanging wall (~91.6%), but lower in the footwall (~82.2%).

These data define a proximal chlorite-carbonate-pyrite zone (high CCPI, high Fe) centered on the ore, surrounded by a more sericite-rich envelope (high ISER, high AI) preferentially developed in the footwall. The asymmetric alteration style is associated with upward fluid flow within more porous sandy strata, and strain localization in D_2 shear zones. Figure 8 shows the AI-CCPI Box Plot graph, which proves that the alteration intensity rises towards high-strain faults. The CCPI/AI ratio is highest in the ore (5.5), moderate in the hanging wall (1.7), and lowest in the footwall (1.2). Such a direct relationship implies that D_2 shear strains and D_4 fault reactivations constantly increased permeability, allowing the flow of iron-magnesium-rich fluids into and surrounding the massive sulfides, whereas sericitization fluids formed the distal halos. High CCPI levels in relation to moderate AI values suggest a reliable proxy for "near-ore, high-strain," while high AI and ISER values denote the distal sericite-rich footwall.

Paragenesis and metal dispersal in deformed VMS deposits

Petrological and X-ray diffraction analysis has confirmed that both hanging wall pelites, as well as the footwall sandy pelites were subjected to greenschist facies metamorphism. Apart from the existing textures and assemblages of minerals, micromesoscopic relations have revealed that the metallogenic process took place through a three-stage evolution associated with deformation (see Figure 12). In particular, the first stage refers to syngenetic accumulation of iron-rich sulfides (Po ± Py ± Cpy) within the volcanosedimentary basin. The second stage is associated with syn-foliation metallogenic processes involving boudinage, transposition, and veining along high strain shear zones to form local copper-zinc mineralization. The third stage refers to post-foliation infilling of Cpy-Sph-Py-Gn assemblages within fractures and shear zones formed due to late deformation stages D_3-D_4.

Data obtained from geochemical and mineralogical studies of drilling core samples corroborate this sequence with vertical zonation of metals: iron-bearing core, zinc-lead bearing upper zone, and copper pockets related to shear zones.

Synthesis and genetic model

Taken together, the Central Block records a syngenetic VMS system substantially reworked by polyphase Variscan deformation. The tripartite architecture footwall sandy pelites → massive sulfide lenses → hanging-wall black pelites is genuine, although lens margins and internal fabrics are extensively structurally overprinted. D1-D2 shortening and shearing duplicated and segmented these horizons by boudinage, folding, and transposition, while D4 brittle stepovers laterally offset them. In vertical sections, this segmentation can appear as one, two, or three discrete lenses depending on drill azimuth and intersection angle.

This model explains: (i) why DF462 and DF453 intersect what is effectively the same lens in different structural positions; (ii) why DF469 shows disc-like massive intervals separated by deformed hanging-wall pelites, although field relations indicate a single folded-sheared lens crossed twice; and (iii) why grades vary strongly within and between lenses, with Fe-rich cores, Zn-Pb-rich upper segments, and Cu-bearing pockets pinned to shear/fracture-controlled permeability.

Integrating the three-unit stratigraphy (volcanosedimentary footwall, massive sulfide lenses, pelitic hanging wall), polyphase deformation (pervasive S1, ductile shears, S2 crenulation, late brittle faults), alteration zoning (proximal chlorite/CCPI, distal sericite/ISER with AI > 40% in the footwall), and a three-stage paragenesis, the Central Block is best viewed as a

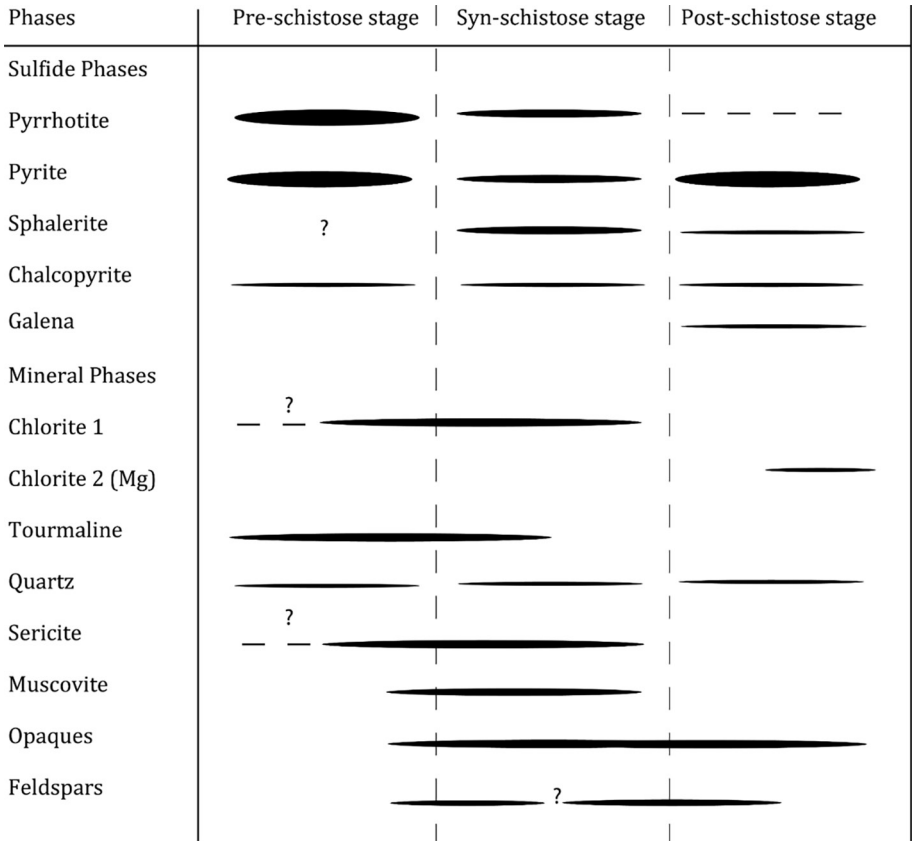

Figure 12. Paragenetic sequence of Draâ Sfar VMS deposits

syngenetic VMS subsequently partitioned and remobilized by Variscan tectonics. Either the presence of a sole lens with branches extending to the north or multiple lenses being deposited initially would be viable interpretations, with the latter case depending on the presence of primary volcanic-sedimentary heterogeneity and secondary boudinage/shearing leading to fracturing and replication of ore structures. Generally speaking, the tectonometallogenic history of the Draâ Sfar deposit conforms to a Variscan age observed in the rest of the Jebilet-Guemassa belt and the larger Hercynian regions (Mrini et al., 1992; Marcoux et al., 2008; Moreno et al., 2008; Lazreq et al., 2021). Syngenesis is considered to have taken place in a Devonian-Carboniferous extensional basin followed by Variscan folding of the mineralization.

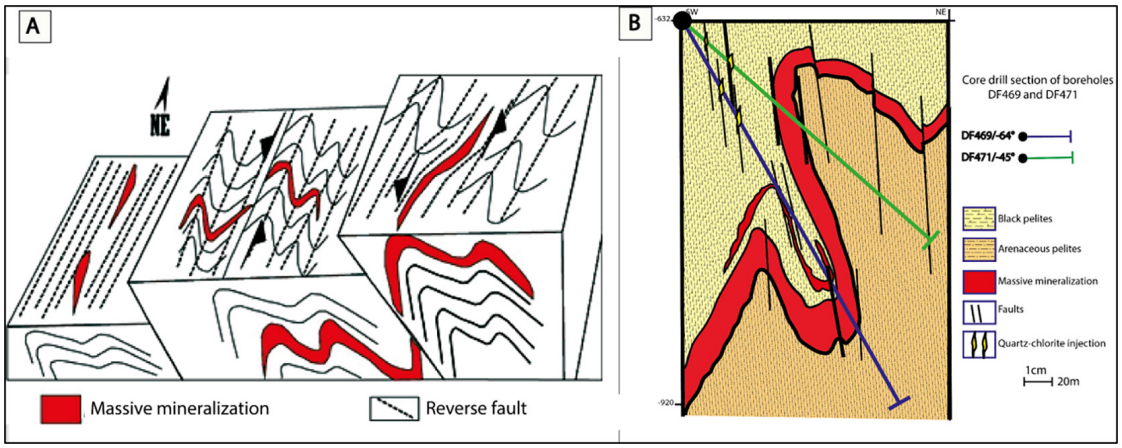

Figure 13. A) Closure phase of the Jebilet Basin and deformation of Draâ Sfar (after Hibti 2001) B) Interpretative section of core drill holes DF469 and DF471

Several large-sized massive sulphides, like Kettara, Hajjar, Koudiat Aïcha, and Draâ Sfar North, in the Jebilet-Guemassa district can be found in association with volcano-sedimentary sequence, showing similar deformational and fluid mobility features during the Variscan deformation event as well, implying regional association of deformed VMS deposits (Leblanc, 1993; Essaifi et al., 2019). Similar occurrences have been reported for other major VMS belts associated with the Variscan Orogeny, for example, the Iberian Pyrite Belt (Neves Corvo and Rio Tinto) (Pereira et al., 2021; de Mello et al., 2022; León et al., 2023; Martín-Méndez et al., 2023; Sáez et al., 2024), where some of the largest volcanogenic massive sulphides have been generated in syn-volcanic settings and later reworked due to tectonic deformations.

CONCLUSIONS

The combination of data on the lithology, structure, petrography, geochemistry, and metallogeny of the central block of the Draâ Sfar deposit allows for the identification of a system of deformed syngenetic volcanogenic massive sulphide deposits. The massive sulfide deposits located between the sandy pelites of the lower wall and the black pelites of the upper wall initially formed in an extensional basin during the Devonian-Carboniferous period, under conditions favorable to the development of Fe-Cu-Zn-Pb sulfides. Variscan compressional deformation led to the formation of a ubiquitous S1 schistosity, ductile D2 shear zones, and brittle faults that reoriented the S1/P1 structures, initially oriented in the NE main trend, toward the NNE, fragmenting and duplicating the initial mineralized zones.

Local remobilization during deformation and metamorphism is evidenced by the presence of massive, iron-rich pyrrhotite nuclei, upper zones rich in Zn-Pb, and shear-related vein deposits rich in Cu. Fluid-rock interaction is also seen through zonation related to hydrothermal alteration in the form of chlorite, carbonate, and pyrite alteration within the zone close to mineralization, characterized by high CCPI. Sericite zonation downstream from mineralization shows high ISER and AI values. High values of CCPI/AI are also seen in shear zones, and this implies that deformation has enhanced permeability.

Acknowledgements

This research is part of a tectono-metallogenic study of the central Draa Sfar virgin area. The authors sincerely thank the Mining Company (CMG) for funding the analyses and for the valuable support provided by its staff during the fieldwork. This study was conducted at the Faculty of Sciences Chouaïb Doukkali in El Jadida and at the Draa Sfar mining site. The authors also thank the Reminix Laboratory in Marrakech for ICP geochemical analyses and for the preparation of thin sections and polished sections, the geology service of the Draa Sfar mining site, the Department of Geology in El Jadida, and the DX platform of the Department of Chemistry in El Jadida for powder preparation and XRD analyses.

REFERENCES

1. Barrakad, A., Huvelin, P., Laforet, C. (1977). Mineraux de cobalt, d'etain, de bismuth, de selenium, d'or et d'argent dans l'amas sulfure a pyrrhotite de Sidi-Embarek (Jebilet). *Notes et Memoires du Service Géologique du Maroc, 37*, 129–138.
2. Ben aissi, L. (2008). *Contribution à l'étude gîtologique des amas sulfu- rés polymétalliques de Draa Sfar et de Koudiat Aïcha: compa- raison avec les gisements de Ben Slimane et de Kettara (Jebilet centrales, Maroc Hercynien).* Thèse Doct. Etat Univ. Cadi Ayyad, Marrakech, 334 p.
3. Bouloton, J. (1992). Mise en évidence de cordiérite héritée des terrains traversés dans le pluton granitique des Oulad Ouaslam (Jebilet, Maroc). *Canadian Journal of Earth Sciences, 29*, 658–668.
4. Bouloton, J., Gasquet, D. (1995). Melting and undercooled crystallisation of felsic xenoliths from minor intrusions (Jebilet massif, Morocco). *Lithos, 35*, 201–219.
5. de Mello,C.R., Tornos, F., Conde, C. (2022). Geology, geochemistry, and geochronology of the giant Rio Tinto VMS deposit, Iberian Pyrite Belt, Spain. *Economic Geology, 117*, 1149–1177.
6. Essaifi, A., Ballèvre, M., Marignac, C., Capdevila, R. (2001). Découverte et signification d'une paragenèse à ilménite zincifère dans les métapélites des Jebilet centrales (Maroc). *Comptes Rendus de l'Académie des Sciences-Series IIA-Earth and Planetary Science, 333*, 381–388.
7. Essaifi, A., Capdevila, R., Lagarde, J. (2004). Metasomatic trondhjemites and tonalites: examples in Central Jebilet (Hercynian, Morocco). *Journal of African Earth Sciences, 39*, 369–374.

8. Essaifi, A., Goodenough, K., Tornos, F. (2019). The Moroccan massive sulphide deposits: evidence for a polyphase mineralization. *Minerals, 9*, 156. https://doi.org/10.3390/min9030156
9. Gaboury, D. (2004). *Paramètres des alterations hydrothermales des gisements de type VMS et aurifères : Comparaison de la performance d'indicateurs d'altération*', Public report, CONSOREM, Que., Canada, available at: www.consorem.ca/production_scien/alterations_hydrothermales.pdf
10. Hibti, M. (2001). Les amas sulfurés des Guemassa et des Jebilet (Meseta Sud Occidentale, Maroc): Témoins de l'hydrothermalisme précoce dans le bassin mésétien. Doctorat d'Etat ès-Sciences, Faculté des Sciences, Marrakech.
11. Huvelin, P. (1977). *Etude Geologique et Gitologique Du Massif Hercynien Des Jebilet (Maroc Occidental).* Tectonics.
12. Lagarde, J.L. (1985). Cisaillements ductiles et plutons granitiques contemporains de la déformation hercynienne post viséenne de la méséta marocaine. *Bulletin de la Société Géologique et Minéralogique de Bretagne, 1*, 29–37
13. Lagarde, J.L., Capdevila, R., Fourcade, S. (1992). Granites et collision continentale: l'exemple des granitoïdes carbonifères dans la chaîne hercynienne ouest-européenne. *Bulletin-Societe Geologique de France, 163*, 597–597.
14. Lazreq, N., Königshof, P., Essaifi, A. (2021). A Devonian age for the Sarhlef Formation (Jebilet Massif, Morocco)–evidence from new biostratigraphic data based on metamorphosed conodonts. *Palaeogeography, Palaeoclimatology, Palaeoecology, 572*, 110395.
15. Leblanc, M. (1993). *Amas sulfuré formé par injection de sills dans des sédiments: exemple d'Hajar (Marrakech, Maroc).* Comptes rendus de l'Académie des sciences Série 2, Mécanique, Physique, Chimie, Sciences de l'univers, Sciences de la Terre, 316, 499–504.
16. León, R., Macías, F., Cánovas, C.R. (2023). Evidence of rare earth elements origin in acid mine drainage from the Iberian Pyrite Belt (SW Spain). *Ore Geology Reviews, 154*, 105336
17. Leprêtre, R., Villeneuve, M., Chopin, F. (2024). *The Variscides in the NW Corner of Africa.* In: The Geology of North Africa. Springer: 145–185.
18. Marcoux, E., Belkabir, A., Gibson, H.L. (2008). Draa Sfar, Morocco: A Visean (331 Ma) pyrrhotite-rich, polymetallic volcanogenic massive sulphide deposit in a Hercynian sediment-dominant terrane. *Ore Geology Reviews, 33*, 307–328. https://doi.org/10.1016/j.oregeorev.2007.03.004
19. Martín-Méndez, I., Llamas Borrajo, J., Bel-lan, A., Locutura, J. (2023). Geochemical distribution in residual soils of Iberian Pyrite Belt (Spain). *Journal of Iberian Geology, 49*, 97–114.
20. Michard, A. (1976). *Eléments de géologie marocaine. Notes et Mémoires du Service géologique du Maroc, n° 252,* Éditions du Service géologique du Maroc, Rabat, Maroc, 408.
21. Michard, A., Soulaimani, A., Hoepffner, C. (2010). The south-western branch of the Variscan Belt: evidence from Morocco. *Tectonophysics, 492*, 1–24.
22. Moreno, C., Sáez, R., González, F. (2008). Age and depositional environment of the Draa Sfar massive sulfide deposit, Morocco. *Miner Deposita, 43*, 891–911. https://doi.org/10.1007/s00126-008-0199-x
23. Mrini, Z., Rafi, A., Duthou J.L,. Vidal, P. (1992). Chronologie Rb-Sr des granitoides hercyniens du Maroc; consequences. *Bulletin de la Société géologique de France, 163*, 281–291.
24. Pereira, Z., Matos, J.X., Solá, A.R. (2021). Geology of the recently discovered massive and stockwork sulphide mineralization at Semblana, Rosa Magra and Monte Branco, Neves–Corvo mine region, Iberian Pyrite Belt, Portugal. *Geological Magazine, 158*, 1253–1268.
25. Pouclet, A., El Hadi, H., Bardintzeff, J.M. (2017). Devonian to Early Carboniferous magmatic alkaline activity in the Tafilalt Province, Eastearn Morocco: An Eovariscan episode in the Gondwana margin, north of the West African Craton. *Journal of African Earth Sciences, 129*, 814–841.
26. Saber, H, (1998). *Le Stéphano-Permien du Haut Atlas occidentale: étude géologique et évolution géodynamique (Maroc),* PhD Thesis, Université Chouaïb Doukkali, Faculté des Sciences, El-Jadida, Maroc, 212 pp.
27. Sáez, R., González, F., Donaire, T. (2024). Updating geological information about the metallogenesis of the Iberian Pyrite Belt. *Minerals 14*, 860.
28. Yaagoub, D., Hinaje, S., El Fartati, M. (2023). Analyse structurale et reconstitution des paléochamps de contraintes tardi-hercyniens dans la boutonnière d'Aouli (massif de la Haute Moulouya, Maroc). *Estudios Geológicos, 79*, e149.
29. Zouicha, A., Saber, H., Attari, A.E. (2022). Late Hercynian tectonic evolution of the Jebilet Massif (Western Meseta, Morocco) based on tectono-sedimentary analyses of related Permian continental deposits. *Journal of Iberian Geology, 48*, 377–403.